THE JOURNAL OF PHYSICAL CHEMISTRY B

ARTICLE

pubs.acs.org/JPCB

A Time-Dependent Approach to Electronic Transmission in Model Molecular Junctions

N. Renaud,*,† M. A. Ratner,*,† and C. Joachim*,‡

†Department of Chemistry, Northwestern University, 2145 Sheridan Road, Evanston, Illinois 60208-3113, United States

‡Nanoscience Group & MANA Sattelite CEMES/CNRS, 29 rue J. Marvig, BP 4347, 31055 Toulouse Cedex, France

ABSTRACT: We present a simple method to compute the transmission coefficient of a quantum system embedded between two conducting electrodes. Starting from the solution of the time-dependent Schrodinger equation, we demonstrate the relationship between the temporal evolution of the state vector, $|\psi(t)\rangle$, initially localized on one electrode and the electronic transmission coefficient, $T(E)$. We particularly emphasize the role of the oscillation frequency and the decay rate of $|\psi(t)\rangle$ in the line shape of $T(E)$. This method is applied to the well-known problems of the single impurity, two-site systems and the benzene ring, where it agrees with well-accepted time-independent methods and gives new physical insight to the resonance and interference patterns widely observed in molecular junctions.

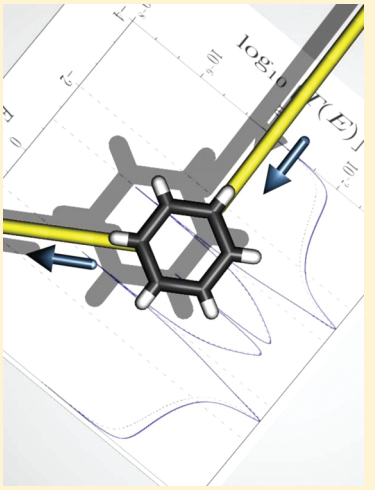

I. INTRODUCTION

Molecular electronics[1] has become an intense field of research following the suggestion of the first molecular rectifier in the mid 1970s.[2−4] To propose an alternative solution to silicon-based circuits, several propositions have been made to implement a Boolean function using the electronic conduction of a single molecule, either utilizing the molecule like a classical circuit[5−8] or using its internal degrees of freedom.[9−14]

Many methods have thus been proposed to compute the elastic conductance of a single molecule when connected to several leads.[15,16] Following the Lippman−Schwinger approach,[17] most of them are based on the solution of the time-independent Schrodinger equation to compute the transmission coefficient, noted T, between electronic eigenstates of the two electrodes. The low-bias current flowing from one electrode to the other is then obtained using the Landauer−Buttiker formula.[18] Several methods can then be used to compute this electronic transmission through a molecular junction. The electron scattering quantum chemistry (ESQC) method, developed by Sautet et al.,[19−21] is based on the transfer matrix formalism where the molecular states are mapped at the end onto each electrode and where the continua formed by the periodic electrodes are exactly treated using spatial propagators. This powerful method allows one, for example, to predict and analyze images obtained via scanning tunnelling microscopy.[22−24] Later, Mujica et al. proposed a Green-function-based method applied to the Lowdin partitioning of the system where the self-energies of the electrodes shift the diagonal matrix element of the molecular Hamiltonian.[25,26] Many other Green-function-based methods have been proposed[28−35] and compared with ESQC[36] that can itself be re-expressed in terms of surface Green functions.[37] Very different approaches can be implemented to compute the transmission matrix such as the recent graph-theoretical-based method proposed by Pickup et al.[38] that uses a source/sink potential to model the electrodes.[39] However, starting from a time-independent point of view, a clear physical interpretation in terms of electron trajectories is hard to obtain from these methods. This interpretation, helpful to understand the mechanism underlying the interference patterns observed in molecular junctions,[40−42] can be made afterward studying the residue of the Green function,[43] converting the transmission coefficient to a rate expression for electron transfer,[44−46] or decomposing the transmission matrix into local contributions.[47]

A formulation of the transmission coefficient from the time-dependent Schrodinger equation could *a priori* give a complete description of the electron trajectory during the tunnelling process and would provide an intuitive interpretation of the resonance and interference patterns observed in a molecular junction. Bar-Joseph et al. proposed such an approach but only for a single quantum state trapped between the two electrodes

Special Issue: Shaul Mukamel Festschrift

Received: November 30, 2010
Revised: January 12, 2011
Published: February 16, 2011

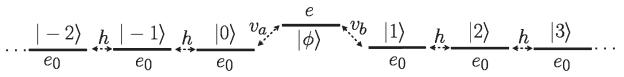

Figure 1. Tight binding model of a single-state impurity, $|\phi\rangle$, embedded between two conducting electrodes. The site energy of each site in the electrode is e_0, and the site−site coupling between two neighboring states is h. The last state of each electrode interacts with the impurity through the coupling strength ν_a and ν_b.

and without comparing their results to previous theory nor studying the behavior of the wave vector during the tunnelling process.[48] Ness et al. also proposed a time-dependent point of view but expressed their result in terms of Green functions, preventing a different interpretation from those obtained with time-independent methods.[49] Recently, Sanchez et al.[50] and Subtonik et al.[51] proposed independently similar solutions based on the steady states of the Liouville equation where the continua formed by the electrodes act as relaxation terms on a small number of bath states interacting with the molecule. Other time-dependent methods have been proposed,[52−57] but to the best of our knowledge, none of them has been used to understand the nature of resonance and interference patterns and their relationship with the evolution of the time-dependent state vector of the system during the tunnelling process.

We propose here a simple model to compute the conductance of a molecular junction starting from the time-dependent Schrodinger equation where the continua formed by the electrodes are described by a Fano model.[58−62] Our solution is compared to time-independent methods for validation and to time-dependent quantities to give physical insight into the conductance line shape. The article is organized as follows: In section II, we present the method when applied to thesingle impurity problem where analytical expressions for all the time-dependent populations can be derived. The concept of resonance is discussed here. The generalization of the method to larger systems is then presented in section III using a Bloch criterion[63−65] to obtain accurate approximative solutions for the evolution of the state vector. In section IV, we study different configurations of two-site systems and give physical insight into the different interference patterns observed. Finally, in the last section, our method is applied to the π network of a benzene ring where the interference and resonance patterns are easily explained using the concepts established in the previous sections.

II. ANALYTICAL CASE: THE SINGLE IMPURITY PROBLEM

We begin with the system represented in Figure 1 where two identical linear chains composed of N states each interact through a single quantum state, $|\phi\rangle$.[66,67] We suppose that only the last site of each electrode interacts with $|\phi\rangle$ though a ν_i coupling. This system has been widely studied, so previous results will help to confirm our own. Consider the solution of the time-dependent Schrodinger equation (taking $\hbar = 1$):

$$|\psi(t)\rangle = e^{-i\mathscr{H}t}|\psi_a\rangle \tag{1}$$

where $\mathscr{H}$ is the Hamiltonian of the entire system describing the two electrodes and the impurity. The initial state, $|\psi_a\rangle$, is chosen as an eigenstate with an energy E of the left electrode. The choice of this particular $|\psi_a\rangle$ is discussed below. Due to the interaction between the left electrode and the impurity, $|\psi_a\rangle$ is not an eigenstate of $\mathscr{H}$. Therefore, the time-dependent state vector, $|\psi(t)\rangle$, can propagate and eventually reach a state at least largely localized in the right electrode. Since we are interested in elastic tunnelling, the target state, labeled $|\psi_b\rangle$, is chosen as an eigenstate of the right electrode with the same energy, E, as $|\psi_a\rangle$.

The coupling strengths ϑ_a, between $|\phi\rangle$ and $|\psi_a\rangle$, and ϑ_b, between $|\phi\rangle$ and $|\psi_b\rangle$, are dominant features in the characteristics of $|\psi(t)\rangle$. With the simple electrodes used here, these couplings are[26,67]

$$\vartheta_i = \eta\nu_i\sqrt{1 - \left(\frac{E - e_0}{2h}\right)^2} \tag{2}$$

with $\eta = (2/(N+1))^{1/2}$, where N is the number of states in the electrode. e_0 and h are, respectively, the energy of each site and coupling strength between two neighboring sites in the electrode (see Figure 1) and are set in the following to $e_0 = 0$ eV and $h = -2$ eV. Therefore, even if the impurity interacts strongly with the electrodes, ϑ_a and ϑ_b remain very weak due to the delocalization of $|\psi_a\rangle$ and $|\psi_b\rangle$ over the large number, N, of sites in each electrode.

To describe the two quasi-continua formed by the electrodes in a finite way, we will use the Fano model[58−60] and the effective Hamiltonian it leads to.[61,62] In this effective Hamiltonian, the energy of any state interacting with one electrode is shifted by an imaginary quantity. This non-Hermitian modification of the Hamiltonian accounts for the wave function leaking in the quasi-continuum through the impurity. Since $|\phi\rangle$ interacts with the two continua, its energy is shifted by $\Gamma = (\Gamma_a + \Gamma_b)$, with $\Gamma_i = -2\nu_i^2\rho(E)$, where $\rho(E) = |1/2h|(1 - ((E-e_0)/2h)^2)^{1/2}$ is the electrode's density of states.[67] The effective Fano Hamiltonian of the system shown in Figure 1 is finally given by

$$\mathscr{H}_{\text{eff}} = \begin{array}{c} \begin{matrix} |\psi_a\rangle & |\psi_b\rangle & |\phi\rangle \end{matrix} \\ \begin{pmatrix} E & 0 & \vartheta_a \\ 0 & E & \vartheta_b \\ \vartheta_a & \vartheta_b & E+e \end{pmatrix} \end{array} + i \begin{array}{c} \begin{matrix} |\psi_a\rangle & |\psi_b\rangle & |\phi\rangle \end{matrix} \\ \begin{pmatrix} 0 & 0 & 0 \\ 0 & 0 & 0 \\ 0 & 0 & \Gamma \end{pmatrix} \end{array} \tag{3}$$

This effective Hamiltonian, sketched in Figure 2, is equivalent to the one derived by Mujica et al., if we only consider the imaginary part of the continuum's self-energy.[25,26] Using this effective Hamiltonian, it is possible to solve eq 1 exactly and to give analytical expressions for the projected wave vector on the different states: $\mathscr{C}_a(t) = \langle\psi_a|\psi(t)\rangle$, $\mathscr{C}_b(t) = \langle\psi_b|\psi(t)\rangle$, and $\mathscr{C}_\phi(t) = \langle\phi|\psi(t)\rangle$

$$\mathscr{C}_a(t) = \frac{\vartheta_a^2}{(\vartheta_a^2 + \vartheta_b^2)}\left(\vartheta_b^2/\vartheta_a^2 + \cos^2\theta e^{-i(e+X_+/2)t}e^{(\Gamma - X_-/2)t} + \sin^2\theta e^{-i(e - X_+/2)t}e^{(\Gamma+X_-/2)t}\right)e^{-iEt} \tag{4}$$

$$\mathscr{C}_b(t) = \frac{-\vartheta_a\vartheta_b}{(\vartheta_a^2 + \vartheta_b^2)}\left(1 - \cos^2\theta e^{-i(e+X_+/2)t}e^{(\Gamma - X_-/2)t} - \sin^2\theta e^{-i(e - X_+/2)t}e^{(\Gamma+X_-/2)t}\right)e^{-iEt} \tag{5}$$

$$\mathscr{C}_\phi(t) = {}^1/_{\sqrt{2}}\cos\theta\sin\theta\left(e^{-i(e+X_+/2)t}e^{(\Gamma - X_-/2)t} - e^{-i(e - X_+/2)t}e^{(\Gamma+X_-/2)t}\right)e^{-iEt} \tag{6}$$

dx.doi.org/10.1021/jp111384d |J. Phys. Chem. B 2011, 115, 5582–5592

The angle θ comes from the definition of the $SU(3)$ matrix which diagonalizes the Hamiltonian given by eq 3 and is given by

$$\theta = \sin^{-1}\left(\frac{\left|E - \frac{e+X_+}{2} - i\frac{\Gamma - X_-}{2}\right|}{\sqrt{\left|E - \frac{e+X_+}{2} - i\frac{\Gamma - X_-}{2}\right|^2 + \delta^2}}\right) \quad (7)$$

with $\delta = (\vartheta_a^2 + \vartheta_b^2)^{1/2}$ and

$$X_\pm = \left[\frac{1}{2}\left(\sqrt{(e^2 - \Gamma^2 + 4\delta^2)^2 + 4e^2\Gamma^2} \pm (e^2 - \Gamma^2 + 4\delta^2)\right)\right]^{1/2} \quad (8)$$

The transmission coefficient, T, that the initial state localized in the left electrode reaches the right electrode is defined by the temporal mean value of $\mathcal{C}_b(t)$ given by eq 5. A major simplification can be made here. Due to the weak value of ϑ_a and ϑ_b, the definition of θ leads to $\theta \simeq \pi/2$. An accurate approximate expression for $\mathcal{C}_b(t)$ can then be obtained neglecting the weak $\cos^2\theta$ term, leading to

$$\mathcal{C}_b(t) \simeq a(1 - e^{-i\Omega t}e^{\Delta t}) \quad (9)$$

with $a = \vartheta_a\vartheta_b/(\vartheta_a^2 + \vartheta_b^2)$, $\Omega = 1/2(|e| - X_+)$, and $\Delta = 1/2\text{-}(\Gamma + X_-) \leq 0$. The very weak values of ϑ_a and ϑ_b act as a filter on $\mathcal{C}_b(t)$ keeping only the dominant Fourier components. Using eq 9, the integral of $\mathcal{C}_b(t)$ does not converge. To solve this problem, the finite lifetime of $|\psi(t)\rangle$ due to relaxation of the wave vector within the electrodes is often introduced.[17,66] Supposing that this lifetime follows an exponential law with rate parameter γ, the temporal mean value of $\mathcal{C}_b(t)$ is given by

$$\langle \mathcal{C}_b(t)\rangle = \int_0^\infty \gamma e^{-\gamma t}\mathcal{C}_b(t)\,dt = a\frac{(\Omega + i\Delta)}{(\Omega + i\Delta) - i\gamma} \quad (10)$$

The same transformation has been used by Ness et al.[49] to compute the mean value of $|\mathcal{C}_b(t)|^2$, where they justify the introduction of the exponential term as a convergence requirement. The electronic transmission coefficient from $|\psi_a\rangle$ to $|\psi_b\rangle$ is then given by $T = |\langle \mathcal{C}_b(t)\rangle|^2$ and reads

$$T = a^2 \cdot \frac{\Omega^2 + \Delta^2}{\Omega^2 + \Delta^2 + \gamma(\gamma - 2\Delta)} \quad (11)$$

It is possible to extract the value of γ from physical arguments, imposing the resonance condition $T(E = e) = 1$. To simplify this derivation, we impose $E = 0$ as the reference energy and suppose the system in the tunnelling regime, i.e., $|h| \gg |\nu_i|$. In this regime, the transmission coefficient is approximated by $T = (a/\gamma)^2(\Omega^2 + \Delta^2)$. This approximation is justified by the rapid decay of Ω and Δ off resonance. With these approximations and after some lengthy algebra, eq 11 becomes

$$T(e) = \frac{1}{\gamma^2}\frac{\vartheta_a^2\vartheta_b^2}{e^2 + \Gamma^2} \quad (12)$$

Imposing $T(e = 0) = 1$ leads to

$$\gamma = \left|\frac{\vartheta_a\vartheta_b}{\Gamma}\right| \quad (13)$$

Since eq 13 is independent of the parameters defining the impurity, this expression will also be used for larger systems in the following.

The probability $T(e)$ given by eq 12 is plotted in Figure 3b for $\nu_i = -1/4$ eV and $h = -2$ eV. On the same figure are plotted the

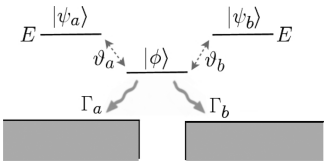

Figure 2. Representation of the Hamiltonian given in eq 3. The initial state, $|\psi_a\rangle$, and the target state, $|\psi_b\rangle$, are eigenstates of the left and right electrode, respectively. These two eigenstates are associated with the same energy E. They both interact with $|\phi\rangle$ through weak couplings ϑ_a and ϑ_b. The interaction between the impurity and the two continua is made by the dissipative Fano terms denoted Γ_a and Γ_b.

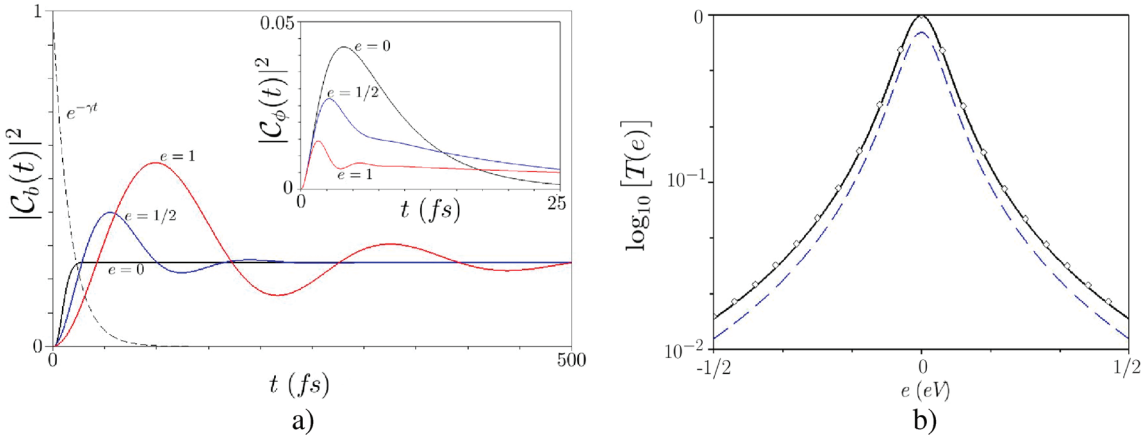

Figure 3. (a) Population of $|\psi_b\rangle$ in the single impurity case for $E = 0$ eV and three values of e: $e = 0$ eV (black), $e = 0.5$ eV (blue), and $e = 1$ (red) eV. The other parameters are as follows: $\nu_a = \nu_b = 0.5$ eV, $h = -2$ eV, and $\eta = 0.2$. During the evolution, half of the population leaks in the continua and the other half oscillates between $|\psi_a\rangle$ and $|\psi_b\rangle$ through $|\phi\rangle$. The transmission coefficient is proportional to the area below $e^{-\gamma t} \times |\mathcal{C}_b(t)|^2$. As shown in the inset, the population of the central state decreases when e moves away from the resonance. (b) Transmission given by eq 12 (plain line), the ESQC method (diamond points), and the Green-function-based method[25,26] (dashed blue line) computed for $h = -2$ eV and $\nu_i = -0.25$ eV.

dx.doi.org/10.1021/jp111384d |J. Phys. Chem. B 2011, 115, 5582–5592

transmission coefficient for the same system calculated with the ESQC method[19] and the Green-function-based method.[25] These three curves present the same Lorentzian shape centered on $E = e$, and very good agreement among the three is seen. Furthermore, the method presented here gives access to important physical quantities such as the population of the different states involved in the electron transfer through the junction. Valuable physical information can be obtained comparing eq 11 to the target state population given by

$$|\mathcal{C}_b(t)|^2 = a^2(1 + e^{2\Delta t} - 2e^{\Delta t}\cos(\Omega t)) \qquad (14)$$

The parameters Ω and Δ, which define the $T(e)$ line shape, are clearly identified as the oscillation frequency and the exponential envelope parameter of the target state population. The oscillation amplitude, a, only modifies the mean value of $T(e)$ but does not affect its profile. This definition of the transmission coefficient agrees with Bardeen's work[68] that proposed a relation between the $T(E)$ and the square of the oscillation frequency between the two reservoirs.

The target state population, $|\mathcal{C}_b(t)|^2$ given by eq 5, is plotted in Figure 3a for $e = 0$, 0.5, and 1 eV with $\eta = 0.2$ and $\nu_a = \nu_b = 0.5$ eV. Due to the dissipative term in the Hamiltonian, half of the population leaks in the continua during the temporal evolution. When the steady state is reached, the other half is equally distributed on $|\psi_a\rangle$ and $|\psi_b\rangle$ and the population of $|\phi\rangle$ is null. This explains why $|\mathcal{C}_b(\infty)|^2$ converges to 1/4 in this particular configuration. This peculiar behavior does not affect the calculation of $T(e)$, since the exponential term $e^{-\gamma t}$ reaches zero rapidly. As already proposed in the literature,[54] only the first oscillations of $\mathcal{C}_b(t)$ are involved in the computation of $T(e)$: the function $\gamma e^{-\gamma t}$ acts as a band-pass filter on the target state population.

In the time-dependent approach depicted above, a resonance in $T(E)$ appears as a maximum oscillation frequency of the target state population, which is obtained here for $e = 0$. At this energy, this oscillation frequency becomes $\Omega(e = 0) = \eta(\nu_a{}^2 + \nu_b{}^2)^{1/2}$, whereas it is proportional to η^2 off resonance. The envelope parameter, Δ, varies also with e. Its absolute value is maximal for $e = 0$ where it becomes $2\delta^2/\Gamma$, whereas it is proportional to δ^4 off resonance. This explains the evolution of the target state population obtained at resonance where the oscillatory term is completely damped by the envelope. At resonance, $|\langle\mathcal{C}_b(t)\rangle|^2$ is maximum and the transmission coefficient presents a peak.

The coefficient $\mathcal{C}_\phi(t) = \langle\phi|\psi(t)\rangle$, given by eq 6, is also a valuable quantity. As can be observed in the inset of Figure 3a, the maximal amplitude of $|\mathcal{C}_\phi(t)|^2$ is larger at resonance than off resonance. This amplitude also increases when the amplitude of the imaginary Fano terms decreases. However, this amplitude remains close to zero which is characteristic of superexchange oscillations between the initial and the target state.[54,15,69]

In a time-dependent calculation, the choice of the initial state is a key feature. An initial state localized on one single atomic orbital of the left electrode[49] or a state uniformly distributed over all these atomic orbitals[55] is often used. In such situations, since the initial state is not an eigenstate of the unperturbed electrode, $|\psi(t)\rangle$ propagates in the left electrode subspace due to strong site−site coupling rather than oscillating smoothly from one electrode to the other. Then, the oscillation amplitude of any state localized in the right electrode remains extremely low, and the definition of a transfer coefficient becomes tricky. Using an eigenstate of the unperturbed left electrode solves this problem and allows us to obtain Rabi-like oscillations of the wave function between the two electrodes. The principal drawback of this specific initial state is the very slow oscillation rate obtained between $|\psi_a\rangle$ and $|\psi_b\rangle$ which is proportional to η and η^2, respectively, at and off resonance. For example, with $\vartheta_a = \vartheta_b = 10^{-1}$ eV, i.e., when $|\psi_a\rangle$ and $|\psi_b\rangle$ are delocalized over roughly 100 orbitals, the time needed for the initial state to be entirely transferred to the target state is around 22 fs at resonance and increases dramatically off resonance.

III. GENERALIZATION TO LARGER SYSTEMS

The same time-dependent analysis can be made for molecules with several sites. Following the same model used above, the Hamiltonian used to compute $T(E)$ is

$$\mathcal{H} = \begin{array}{c} \begin{matrix} |\psi_a\rangle & |\psi_b\rangle & \ldots|\phi_j\rangle\ldots \end{matrix} \\ \left(\begin{array}{cc|c} E & 0 & \\ 0 & E & \boldsymbol{\vartheta}^\dagger \\ \hline & \boldsymbol{\vartheta} & \mathcal{H}_0 + i\boldsymbol{\Gamma} \end{array}\right) \end{array} \qquad (15)$$

where ϑ is a coupling matrix containing the weak coupling strength ϑ_i between $|\psi_a\rangle$, $|\psi_b\rangle$ and the molecular states $|\phi_j\rangle$. $\mathcal{H}_0$ is the unperturbed Hamiltonian of the molecule, and Γ is the dissipative Fano matrix. In the general case, this matrix can contain off-diagonal elements when several molecular states interact with the same electrode.[62]

For these systems, the time-dependent Schrodinger equation cannot generally be solved analytically. Thanks to the small values of the coupling strength between the scattering states and the central molecule in the tunnel junction, a very accurate solution can be easily obtained through a Bloch criterion.[13,63,65] Suppose that the initial and target states are resolved on the eigenbasis of the Hamiltonian by $|\psi_a\rangle = \sum_n a_n|\Psi_n\rangle$ and $|\psi_b\rangle = \sum_n b_n|\Psi_n\rangle$, where $\{\ldots, |\Psi_n\rangle, \ldots\}$ are the eigenvectors of the Hamiltonian. The function $\mathcal{C}_b(t) = \langle\psi_b|e^{-i\mathcal{H}t/\hbar}|\psi_a\rangle$ can then be written as

$$\mathcal{C}_b(t) = \sum_n a_n b_n^* \exp^{-i\lambda_n t} \qquad (16)$$

where λ_n is the nth eigenvalue of the Hamiltonian. Due to the topology of the system, $|\psi_a\rangle$ and $|\psi_b\rangle$ are mainly localized on two eigenstates, labeled $|\Psi_+\rangle$ and $|\Psi_-\rangle$, and associated with the eigenvalues $\lambda_\pm$. Numerically, the two eigenstates $|\Psi_+\rangle$ and $|\Psi_-\rangle$ can be found easily, since they maximize the Bloch criterion:

$$\Lambda_{n,m} = \langle\psi_a|P_n|\psi_b\rangle\langle\psi_b|P_m|\psi_a\rangle \qquad (17)$$

with $P_k = |\Psi_k\rangle\langle\Psi_k|$. The general expression for $\mathcal{C}_b(t)$ can therefore be simplified to

$$\mathcal{C}_b(t) \simeq a_{\text{eff}}(\exp^{-i\lambda_+ t} - \exp^{-i\lambda_- t}) \qquad (18)$$

where $a_{\text{eff}} = \sum_n|a_n b_n|$ is the amplitude of the effective oscillation. The mean value of eq 18 is calculated following the transformation introduced in eq 10, and the transfer coefficient is given by the square modulus of this mean value. With the same approximations used for the single impurity case, $T(E)$ of a multistate system is given by

$$T(E) = a_{\text{eff}}{}^2 \cdot \frac{\Omega^2 + \Delta^2}{\gamma^2} \qquad (19)$$

dx.doi.org/10.1021/jp111384d |J. Phys. Chem. B 2011, 115, 5582–5592

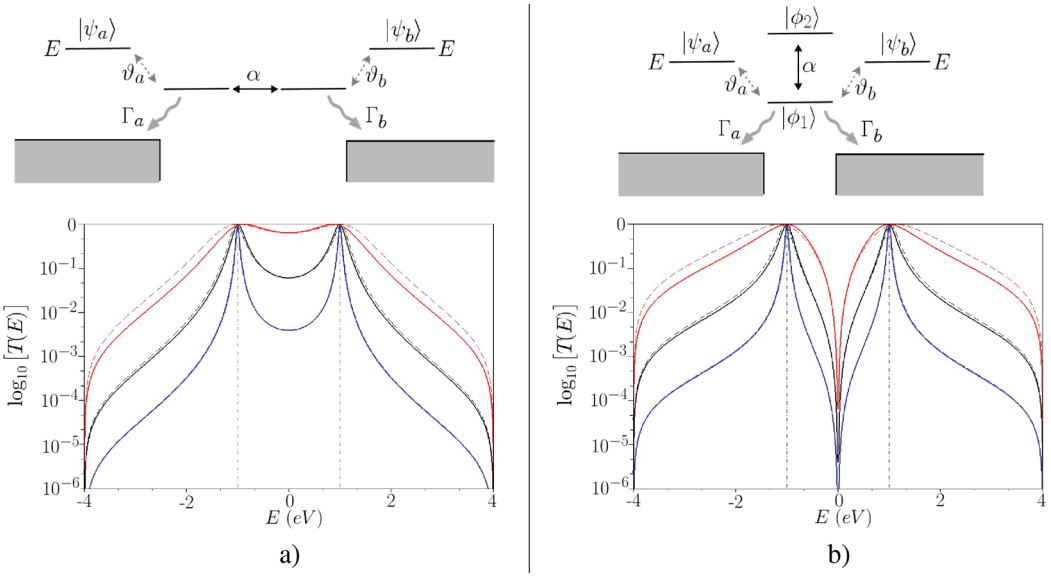

Figure 4. Two-site system in (a) longitudinal and (b) transverse configuration. The electronic transmission of these two systems calculated with our method (plain curves) and the ESQC method (dashed curves). The calculation has been made for $\alpha = -1$ eV and $e_1 = e_2 = 0$ for both cases, even if represented differently in part b. The electrodes are the same as in Figure 1 with $h = -2$ eV. The interactions between the electrodes and the sites are $\nu_a = \nu_b = 0.25$ (blue lines), 0.5 eV (black lines), and 1 eV (red lines). The vertical dashed lines represent the position of the molecular eigenstates.

with γ given by eq 13. In eq 19, Ω and Δ are given by $\Omega = \mathrm{Re}(\lambda_- - \lambda_+)$ and $\Delta = |\mathrm{Im}(\lambda_- - \lambda_+)|$. These parameters are, respectively, the oscillation frequency and the decay rate of $|\mathcal{C}_b(t)|^2 = a_{\mathrm{eff}}^2 e^{-2\Delta t}\sin^2(\Omega t)$. This method provides a black box allowing us to compute the transmission coefficient of any system tracking the dominant subspace formed by the eigenvectors $|\Psi_\pm\rangle$. On the basis of an effective model, this method does not give access to the projection of a wave vector on the different states. These quantities, very useful to understand the patterns in the $T(E)$ line shape, will be approximated using the Dyson expansion of the time-dependent Schrodinger equation.

Two-Site Systems: Interferences. A two-site system, with two states $|\phi_1\rangle$ and $|\phi_2\rangle$ of energies e_1 and e_2, can interact in different ways with the electrodes and therefore can lead to different $T(E)$ line shapes. The longitudinal and transverse situations are represented in Figure 4. Their respective electronic transmissions have been calculated following the method presented in the previous section. The Fano matrices in the longitudinal (Γ_L) and transverse (Γ_T) configuration are, respectively,

$$\begin{array}{c} \\ |\phi_1\rangle \\ |\phi_2\rangle \end{array}\!\!\begin{array}{c} \begin{array}{cc} |\phi_1\rangle & |\phi_2\rangle \end{array} \\ \begin{pmatrix} \Gamma_a & 0 \\ 0 & \Gamma_b \end{pmatrix} \end{array} \quad \begin{array}{c} \\ |\phi_1\rangle \\ |\phi_2\rangle \end{array}\!\!\begin{array}{c} \begin{array}{cc} |\phi_1\rangle & |\phi_2\rangle \end{array} \\ \begin{pmatrix} \Gamma_a+\Gamma_b & 0 \\ 0 & 0 \end{pmatrix} \end{array} \qquad (20)$$

with $\Gamma_i = -2\nu_i^2\rho(E)$. Then, for each value of E, the dominant eigenvalues of the Hamiltonian are computed using the Bloch criteria and then used in eq 19 to compute $T(E)$. The result of this calculation is represented in Figure 4 and compared with the ESQC calculation. Both calculations have been performed using the same electrodes as in Figure 1 with $h = -2$ eV and for different values of ν_a and ν_b. The dimer system used here is characterized by $e_1 = e_2 = 0$ and $\alpha = -1$ eV.Very good agreement between the two methods is seen.

The conduction of the serial configuration is the typical multiple-resonance line shape of a simple two-atom wire. As for the single impurity case, when the energy E is resonant with an eigenenergy, $\lambda_\pm$, of the dimer, the oscillation frequency of $|\mathcal{C}_b(t)|^2$ becomes $\Omega(E = \lambda_\pm) = \eta(\nu_a^2 + \nu_b^2)^{1/2}$ and the transmission coefficient is equal to unity. In between these two values, the oscillation frequency is proportional to η^2 and the transmission decreases dramatically.

Frequency-Related Interference. The transverse configuration presents a deep interference in between the two resonances. While this interference is well-known,[40,44,70] the time-dependent method presented here allows new insight into the physical process leading to this effect. Since this interference appears for any value of the coupling terms, ν_a and ν_b, we study the simplest situation where these couplings are small enough for the imaginary part of the Hamiltonian to be neglected. In this situation and assuming $\vartheta_a = \vartheta_b = \vartheta$, the Hamiltonian of the transverse configuration reads

$$\begin{array}{c} \\ |\psi_a\rangle \\ |\psi_b\rangle \\ |\phi_1\rangle \\ |\phi_2\rangle \end{array}\!\!\begin{array}{c} \begin{array}{cccc} |\psi_a\rangle & |\psi_b\rangle & |\phi_1\rangle & |\phi_2\rangle \end{array} \\ \begin{pmatrix} E & . & \vartheta & . \\ . & E & \vartheta & . \\ \vartheta & \vartheta & e_1 & \alpha \\ . & . & \alpha & e_2 \end{pmatrix} \end{array} = \begin{array}{c} \\ |\psi_a\rangle \\ |\psi_b\rangle \\ |\phi_-\rangle \\ |\phi_+\rangle \end{array}\!\!\begin{array}{c} \begin{array}{cccc} |\psi_a\rangle & |\psi_b\rangle & |\phi_-\rangle & |\phi_+\rangle \end{array} \\ \begin{pmatrix} E & . & \vartheta_- & \vartheta_+ \\ . & E & \vartheta_- & \vartheta_+ \\ \vartheta_- & \vartheta_- & \lambda_- & . \\ \vartheta_+ & \vartheta_+ & . & \lambda_+ \end{pmatrix} \end{array} \qquad (21)$$

with $\lambda_\pm = 1/2[(e_1 + e_2) \pm ((e_1 - e_2)^2 + 4\alpha^2)^{1/2}]$, $\vartheta_- = \vartheta\cos\theta$, and $\vartheta_+ = \vartheta\sin\theta$, where $\theta = 1/2\tan^{-1}[2\alpha/(e_1 - e_2)]$. The dots in eq 21 are null matrix elements not represented to emphasize the structure of the system. Using the Dyson expansion of the time-dependent Schrodinger equation, one can obtain the expression of the projected wave function on the dimer eigenstates, $\mathcal{C}_{\phi_\pm}(t) = \langle\phi_\pm|\psi(t)\rangle$:

$$\mathcal{C}_{\phi_\pm}(t) \simeq \frac{\vartheta_\pm}{\omega_\pm}[(1 - \cos\omega_\pm t) - i\sin\omega_\pm t]e^{iEt} \qquad (22)$$

with $\omega_\pm = E - \lambda_\pm$. The probability amplitude $\mathcal{C}_b(t) = \langle\psi_b|\psi(t)\rangle$, can be obtained using the second order of the

dx.doi.org/10.1021/jp111384d |J. Phys. Chem. B 2011, 115, 5582–5592

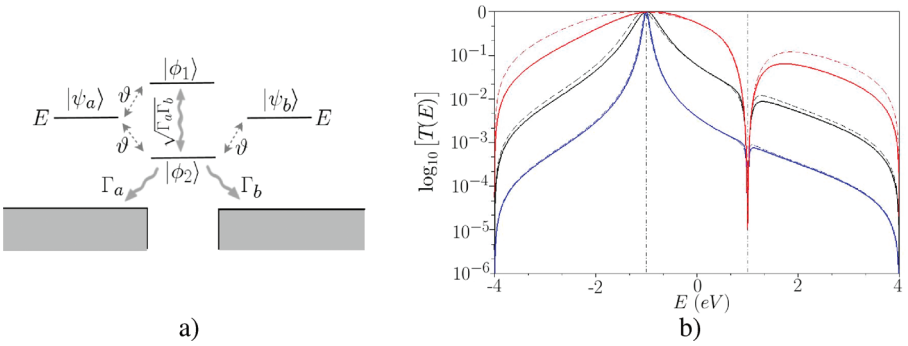

Figure 5. (a) Two-level system with one conductive state ($|\phi_2\rangle$) and one dangling state ($|\phi_1\rangle$). (b) The electronic transmission of this two-level system, calculated with our method (plain) and the ESQC method (dashed). The calculation has been made for $e_1 = -e_2 = 1$ eV. The electrodes are the same as in Figure 1 with $h = -2$ eV and $\nu_i = 0.25$ eV (blue lines), 0.5 eV (black lines), and 1 eV (red lines). The vertical dashed lines represent the energetic position of the two states.

Dyson expansion:

$$\mathscr{C}_b(t) \simeq -i \sum_{n=\pm} \vartheta_n \int_0^t e^{-i\omega_n \tau} \mathscr{C}_n(\tau)\, d\tau$$

$$= \sum_{n=\pm} \frac{{\vartheta_n}^2}{\omega_n} \left[\frac{1 - e^{i\omega_n t}}{\omega_n} + it \right] e^{iEt} \qquad (23)$$

The term $\sum_n (\vartheta_n/\omega_n)^2 (1 - e^{i\omega_n t})$ reflects the presence of high frequency components with a very small amplitude in the development of $\mathscr{C}_b(t)$. The term $\sum_n ({\vartheta_n}^2/\omega_n)t$ is the first-order development of the function $\sin(\sum_n ({\vartheta_n}^2/\omega_n)t)$, which is a low frequency component with amplitude equal to 1. This sinusoidal function smooths $\mathscr{C}_b(t)$ with Rabi-like oscillations. The oscillation frequency of this term is therefore the dominant oscillation frequency used to compute $T(E)$. This frequency is given by

$$\Omega(E) = \sum_{n=\pm} \frac{{\vartheta_n}^2}{\omega_n} = \sum_n \frac{\langle \psi_a | \mathscr{H} | \phi_n \rangle \langle \phi_n | \mathscr{H} | \psi_b \rangle}{E - \lambda_n} \qquad (24)$$

which is the Green function of the dimer projected on the initial and target states used in most of the time-independent methods to compute the electronic conduction.[25,36,37] In the transverse configuration, this term is given by

$$\Omega(E) = \vartheta^2 \left(\frac{E - \lambda_+ \cos^2\theta - \lambda_- \sin^2\theta}{\prod_{n=\pm} (E - \lambda_n)} \right) \qquad (25)$$

Therefore, for $E = \lambda_+ \cos^2\theta + \lambda_- \sin^2\theta$, the dominant oscillation frequency vanishes, leading to an interference pattern in $T(E)$. In the simple case $e_1 = e_2 = 0$, represented in Figure 4, this interference is located at $E = 0$.

Equation 23 is not really convenient to understand what interferes with what to obtain the interference pattern. A more convenient formulation for $\mathscr{C}_b(t)$ can be obtained neglecting the weak high-frequency terms in eq 23, leading to $\mathscr{C}_b(t) \simeq i \sin(\Omega t) e^{iEt}$. Developing $\sin(\Omega t)\mathscr{C}_b(t)$ becomes

$$\mathscr{C}_b(t) \simeq \mathrm{Im}\left[\prod_{n=\pm} \exp\left(i \left(\frac{h_{an}}{\omega_n} \cdot h_{nb} \right) t \right) \right] e^{iEt} \qquad (26)$$

where $h_{an}/\omega_n = \langle \psi_a | \mathscr{H} | \phi_n \rangle / (E - \lambda_n)$ is the oscillation amplitude of $\mathscr{C}_{\phi_n(t)}$ and $h_{nb} = \langle \phi_n | \mathscr{H} | \psi_b \rangle$ is the coupling strength between $|\psi_b\rangle$ and $|\phi_n\rangle$. $\mathscr{C}_b(t)$ appears as the product of oscillating terms, each coming from one eigenstate of the dimer system. The oscillation frequency of the nth term is given by the oscillation amplitude of $\mathscr{C}_{\phi_n}(t)$ multiplied by the interaction strength between $|\psi_b\rangle$ and $|\phi_n\rangle$. For these interferences to occur, it is therefore not required that all the $\mathscr{C}_{\phi_n}(t)$ oscillate in phase, out of phase, or with any phase relation, to obtain the interference, as long as their amplitudes, weighted by the strength with which $|\psi_b\rangle$ includes each oscillation, cancel each other.

Amplitude-Related Interference. Other configurations can be considered to connect two sites to the electrodes. One solution is represented in Figure 5 where $|\phi_2\rangle$ interacts with both $|\psi_a\rangle$ and $|\psi_b\rangle$ whereas $|\phi_1\rangle$ interacts only with $|\psi_a\rangle$. In this case, the Fano matrix is given by

$$\mathbf{\Gamma} = \begin{array}{c} \\ |\phi_1\rangle \\ |\phi_2\rangle \end{array} \begin{array}{c} \begin{array}{cc} |\phi_1\rangle & |\phi_2\rangle \end{array} \\ \begin{pmatrix} \Gamma_a & \sqrt{\Gamma_a\Gamma_b} \\ \sqrt{\Gamma_a\Gamma_b} & \Gamma_a + \Gamma_b \end{pmatrix} \end{array} \qquad (27)$$

with $\Gamma_i = -2\nu_i^2 \rho(E)$. The off-diagonal matrix element comes from the fact that both $|\phi_1\rangle$ and $|\phi_2\rangle$ interact with the left electrode and are therefore indirectly coupled through this continuum.[62] The electronic conduction of this dangling configuration has been calculated using both the method presented above and the ESQC method for $e_1 = -e_2 = 1$ eV with the same electrodes as in Figure.1. Very good agreement appears once again between the two methods, and both show an interference located at $E = e_1$. To understand the origin of this interference, let us write the Hamiltonian of this configuration and its block-diagonalization in the $\{|\psi_a\rangle, |\phi_1\rangle\}$ subspace, with $\vartheta_a = \vartheta_b = \vartheta$:

$$\mathscr{H} = \begin{array}{c} \\ |\psi_a\rangle \\ |\psi_b\rangle \\ |\phi_1\rangle \\ |\phi_2\rangle \end{array} \begin{array}{c} \begin{array}{cccc} |\psi_a\rangle & |\psi_b\rangle & |\phi_1\rangle & |\phi_2\rangle \end{array} \\ \begin{pmatrix} E & . & \vartheta & \vartheta \\ . & E & . & \vartheta \\ \vartheta & . & e_1 & . \\ \vartheta & \vartheta & . & e_2 \end{pmatrix} \end{array} = \begin{array}{c} \\ |\psi_-\rangle \\ |\psi_b\rangle \\ |\psi_+\rangle \\ |\phi_2\rangle \end{array} \begin{array}{c} \begin{array}{cccc} |\psi_-\rangle & |\psi_b\rangle & |\psi_+\rangle & |\phi_2\rangle \end{array} \\ \begin{pmatrix} E_- & . & . & \vartheta_- \\ . & E & . & \vartheta \\ . & . & E_+ & \vartheta_+ \\ \vartheta_- & \vartheta & \vartheta_+ & e_2 \end{pmatrix} \end{array} \qquad (28)$$

with $E_\pm = 1/2[(E + e_1) \pm ((E - e_1)^2 + 4\vartheta^2)^{1/2}]$, $\vartheta_- = \vartheta \cos\mu$, $\vartheta_+ = -\vartheta \sin\mu$, and $\mu = 1/2 \tan^{-1}(2\vartheta/E - e_1)$. Once again, the Dyson expansion of $\mathscr{C}_b(t)$ is very useful to understand

dx.doi.org/10.1021/jp111384d |J. Phys. Chem. B 2011, 115, 5582–5592

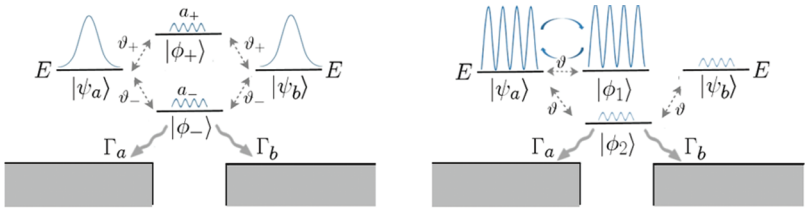

Figure 6. Graphical representation of the two interference patterns observed on the dimer system. (a) Frequency-related interference: the oscillation frequency of $\mathcal{C}_b(t)$ vanishes when $\sum_n a_n \vartheta_n = 0$ with a_n being the oscillation amplitude of $\mathcal{C}_{\phi_n}(t)$. (b) Amplitude-related interference: when $E = e_1$, the initial population is entirely transferred from $|\psi_a\rangle$ to the dangling resonant eigenstate, $|\phi_1\rangle$. The amplitude of $\mathcal{C}_b(t)$ drops then to η^2, whereas it equals 1 when $E \neq e_1$.

the interference pattern observed at $T(E = e_1)$. This expansion leads to

$$\mathcal{C}_b(t) \simeq \left[(\alpha+\beta)\frac{(1 - e^{-i(e_2 - E)t})}{e_2 - E} - \alpha\frac{(1 - e^{-i(E - E_-)t})}{E - E_-} - \beta\frac{(1 - e^{-i(E - E_+)t})}{E - E_+}\right] e^{-iEt} \quad (29)$$

with $\alpha = \vartheta_-{}^2/(E_- - e_1)$ and $\beta = \vartheta_+{}^2/(E_+ - e_1)$. To get a simple picture, let us express $|\mathcal{C}_b(t)|^2$ when $|\phi_1\rangle$ is at and off resonance with E. When $E = e_1$, the population of the target state can be simplified as

$$|\mathcal{C}_b(t)|^2 \simeq \frac{\vartheta^2}{4}\sin^2(\vartheta t) \quad (30)$$

whereas off resonance this population is given by

$$|\mathcal{C}_b(t)|^2 \simeq \left[\frac{1}{2}\frac{E - e_1}{E_- - e_2}\right]^2\left(1 - \cos\left(\frac{2\vartheta^2}{E - e_1}t\right)\right) \quad (31)$$

It is interesting to note that, even if $|\phi_1\rangle$ does not connect the two electrodes, it induces a resonance of $|\mathcal{C}_b(t)|^2$, since its oscillation frequency is maximum at $E = e_1$, where it equals η, and drops to η^2 off resonance. The interference observed at $E = e_1$ is consequently not a frequency-related interference like the one observed in the transverse configuration. On the contrary, the amplitude of $|\mathcal{C}_b(t)|^2$ is minimum at resonance where it scales like η^2 and increases to unity off-resonance. This drastic drop of the oscillation amplitude is responsible for the interference pattern observed at $E = e_1$. The origin of this drop in amplitude is easy to understand writing the Dyson expansion of $\mathcal{C}_{\phi_1(t)}$. Due to the delocalization of $|\psi_a\rangle$ over $|\psi_+\rangle$ and $|\psi_-\rangle$, this expansion contains a zero order term and reads

$$\mathcal{C}_{\phi_1(t)} \simeq 2i\cos\mu\sin\mu e^{-i(E+e_2)/2t}\sin(\omega_0 t) - (\sin\mu\mathcal{C}^{(2)}_{\psi_-}(t) - \cos\mu\mathcal{C}^{(2)}_{\psi_+}(t)) \quad (32)$$

with $\omega_0 = 1/2((E - e_1)^2 + 4\vartheta^2)^{1/2}$ and $\mathcal{C}_{\psi_\pm}{}^{(2)}(t)$ given by the second order of the Dyson expansion terms:

$$\mathcal{C}^{(2)}_{\psi_\pm}(t) = \sum_{n=\pm}\frac{\langle\psi_\pm|\psi_a\rangle\vartheta_n\vartheta_\pm}{E_n - e_2} \times\left(\frac{1 - e^{i(E_\pm + E_n)t}}{E_\pm + E_n} - \frac{1 - e^{i(e_2 - E_\pm)t}}{e_2 - E_\pm}\right) \quad (33)$$

In the vicinity of the resonance, when $E \simeq e_1$, $|\psi_a\rangle$ and $|\phi_1\rangle$ are quasi-degenerate and the zero-order term in eq 32 is far more important than the second-order terms. The population of $|\phi_1\rangle$ then reads

$$|\mathcal{C}_{\phi_1}(t)|^2 \simeq \frac{4\vartheta^2\sin^2(\omega_0 t)}{(E - e_1)^2 + 4\vartheta^2} \quad (34)$$

It is then clear that when $E = e_1$ almost all the initial population is transferred from $|\psi_a\rangle$ to $|\phi_1\rangle$. This leads to the very small oscillation amplitude of $|\mathcal{C}_b(t)|^2$ and consequently to the interference observed in Figure 5. Off resonance, since $E - e_1 \gg \vartheta$, the amplitude of $\mathcal{C}_{\phi_1}(t)$ remains very weak and $|\psi(t)\rangle$ can slowly reach the target state.

The two different types of interferences are schematized in Figure 6, the frequency-related interference where the oscillation frequency of $|\mathcal{C}_b(t)|^2$ drops to 0 and the amplitude-related interference where the oscillation amplitude of $|\mathcal{C}_b(t)|^2$ drops dramatically. The resonance and interference patterns studied for simple pedagogical systems in this section will be very useful in the next section to understand the $T(E)$ line shape of more complex systems.

IV. MOLECULAR JUNCTION: THE BENZENE RING

The resonance and interference patterns studied in the previous sections are widely observed in molecular junctions. Let us examine the well-known case of the π network of a benzene ring between two conducting leads in a tight binding model.[38,40−44,70] In this Huckel-like approximation, the direct coupling between the two electrodes is neglected and therefore does not blur the intrinsic conduction of the molecule. We use the same electrodes as in Figure 1, with $h = -2$ eV; the two electrodes will be connected either in the ortho- or meta-substituted position. These calculations are made for different values of the coupling strength $\nu_a = \nu_b$, which allows us to compare our result with the ESQC calculation in the tunnelling regime ($\nu_i = -0.25$ eV), the pseudoballistic regime ($\nu_i = -2$ eV), and the supercoupled regime ($\nu_i = -4$ eV).

In each configuration, each electrode interacts with a given p_z orbital of the π network of the molecule. The left electrode interacts always with $|\phi_1\rangle$ and the right electrode with $|\phi_X\rangle$ with $X = 2$ in the ortho-configuration, represented in Figure 7a, and $X = 3$ in the meta-configuration. In our model, this leads to a weak coupling between $|\psi_a\rangle$ and $|\phi_1\rangle$ and between $|\psi_b\rangle$ and $|\phi_X\rangle$. The Fano matrix introduces imaginary diagonal elements that shift the energies of $|\phi_1\rangle$ and $|\phi_X\rangle$ by $\Gamma_i = -2\nu_i{}^2\rho(E)$. The transmission coefficient of these two systems has been calculated following the method presented in this article and compared with the

dx.doi.org/10.1021/jp111384d |J. Phys. Chem. B 2011, 115, 5582–5592

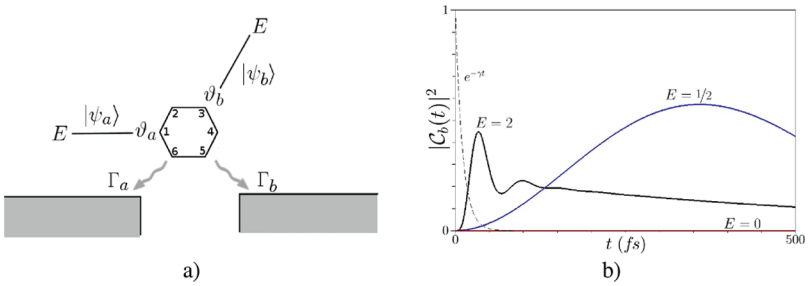

Figure 7. (a) Schematic representation of the system used to compute the transfer coefficient of a benzene ring when the two electrodes are attached in a meta substituted configuration. (b) Population of the target state for different values of E: 2 eV (black), 0.5 eV (blue), and 0 eV (red) with $\eta = 0.25$, $\nu_i = 1/2$ eV, and $h = -2$ eV. In the resonant case, the high oscillation frequency leads to a high conductance, whereas the low oscillation frequency obtained off resonance leads to a low value of the transfer coefficient.

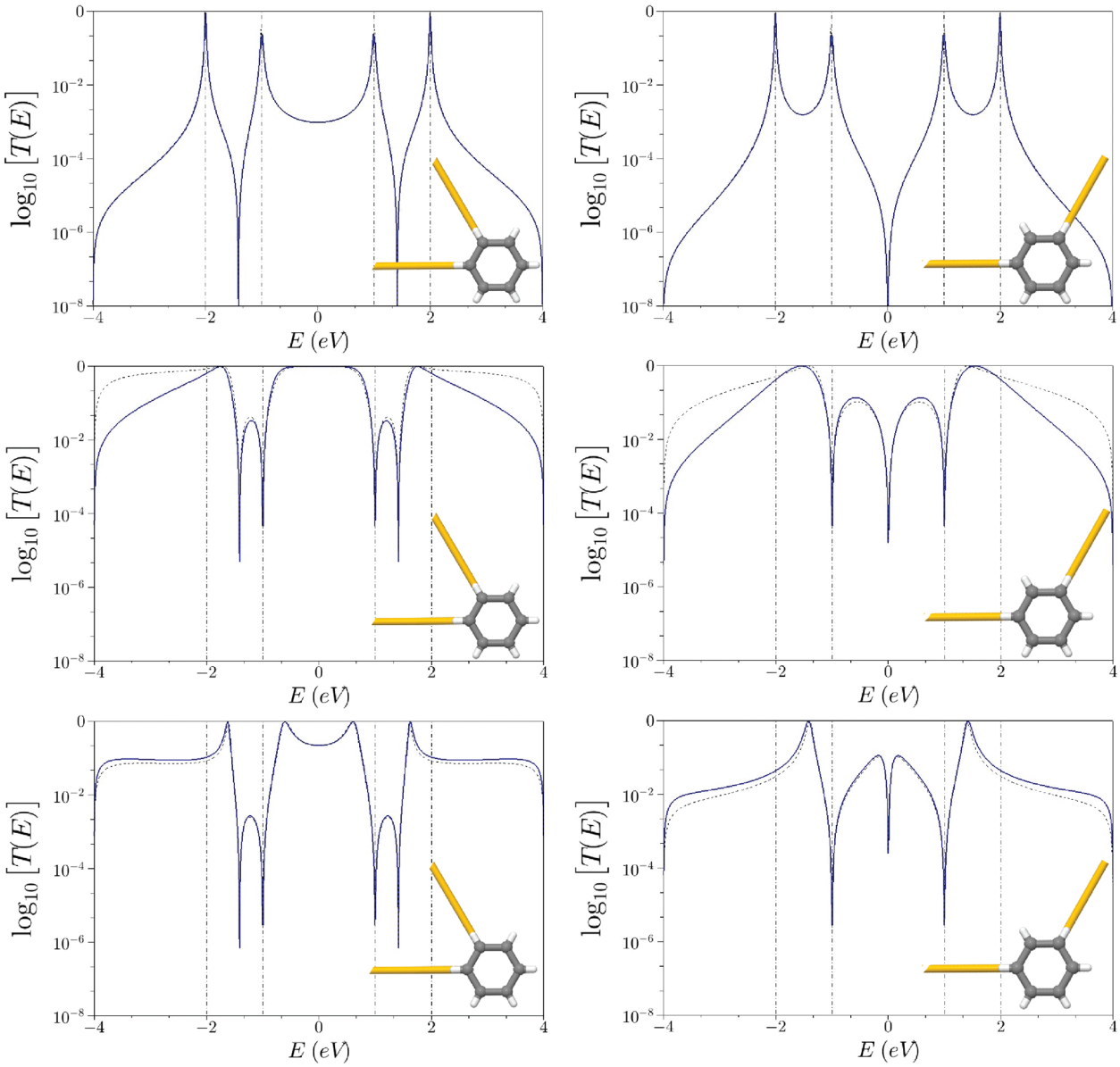

Figure 8. Electronic conduction of a benzene ring in between two conducting electrodes. These calculations are performed by the time-dependent method presented here (solid line) and by the ESQC method (dashed line) for comparison. The electrodes are connected either in ortho (left column) or meta (right column) position. Three regimes are investigated: tunnelling with $\nu_i = -0.25$ eV (top row), pseudoballistic with $\nu_i = -2$ eV (middle row), and supercoupled with $\nu_i = -4$ eV (bottom row). The vertical dashed lines represent the energetic position of the benzene's eigenstates.

dx.doi.org/10.1021/jp111384d |J. Phys. Chem. B 2011, 115, 5582–5592

ESQC calculation. To ease the interpretation, the energy of the p_z orbitals has been set as the reference energy, i.e., 0 eV, and the coupling between two neighboring p_z orbitals normalized to -1 eV. With these parameters, the eigenvalues of the Hamiltonian are simply $e_6 = -e_1 = 2$ eV and $e_5 = e_4 = -e_2 = -e_3 = 1$ eV. As observed in Figure 8, good agreement is found between the two methods for the different values of ν_a and ν_b.

Already observed for the single impurity and the dimer system, the resonances appear clearly and still correspond, as illustrated in Figure 7b, to a maximum of the oscillation frequency reached when E equals the eigenvalues of the benzene π network. As before, resonance corresponds to a maximum of the oscillation frequency between $|\psi_a\rangle$ and $|\psi_b\rangle$.

Interference patterns also appear in both configurations.[40] Several arguments have been made to explain these interferences such as a phase opposition between topological electronic pathways.[44] They have been studied in detail using a Green function formalism[43] and a local current description.[47] The concepts establised in the previous sections are very useful to understand the nature of these interferences. Let us examine the meta-configuration neglecting the imaginary part of the Hamiltonian to facilitate the calulations. Block-diagonalizing the Hamiltonian of the system on the molecular level subspace, the Hamiltonian of the meta-configuration becomes

$$\mathscr{H} = \begin{array}{c} \begin{array}{cccccccc} |\psi_a\rangle & |\psi_b\rangle & |\Psi_1\rangle & |\Psi_2\rangle & |\Psi_3\rangle & |\Psi_4\rangle & |\Psi_5\rangle & |\Psi_6\rangle \end{array} \\ \begin{pmatrix} E & . & \frac{\vartheta}{\sqrt{6}} & -\frac{\vartheta}{\sqrt{12}} & \frac{-\vartheta}{2} & \frac{\vartheta}{2} & \frac{\vartheta}{\sqrt{12}} & \frac{\vartheta}{\sqrt{6}} \\ . & E & \frac{\vartheta}{\sqrt{6}} & \frac{2\vartheta}{\sqrt{12}} & . & . & \frac{-2\vartheta}{\sqrt{12}} & \frac{-\vartheta}{\sqrt{6}} \\ \frac{\vartheta}{\sqrt{6}} & \frac{\vartheta}{\sqrt{6}} & \lambda_1 & . & . & . & . & . \\ -\frac{\vartheta}{\sqrt{12}} & \frac{2\vartheta}{\sqrt{12}} & . & \lambda_2 & . & . & . & . \\ \frac{-\vartheta}{2} & . & . & . & \lambda_3 & . & . & . \\ \frac{\vartheta}{2} & . & . & . & . & \lambda_4 & . & . \\ \frac{\vartheta}{\sqrt{12}} & \frac{-2\vartheta}{\sqrt{12}} & . & . & . & . & \lambda_5 & . \\ \frac{-\vartheta}{\sqrt{6}} & \frac{-\vartheta}{\sqrt{6}} & . & . & . & . & . & \lambda_6 \end{pmatrix} \end{array} \tag{35}$$

where $\{..., |\Psi_n\rangle, ...\}$ are the eigenstates of the benzene ring and $\lambda_1 = -2$ eV, $\lambda_2 = \lambda_3 = -1$ eV, $\lambda_4 = \lambda_5 = 1$ eV, and $\lambda_6 = 2$ eV are its eigenenergies. Two eigenstates, $|\Psi_3\rangle$ and $|\Psi_4\rangle$ associated, respectively, with the energies -1 and 1 eV, are only connected to one of the two electrodes. As for the dimer system, these dangling eigenstates induce amplitude-related interferences when $E = \pm 1$ eV, as seen in Figure 8. The initial population is then completely transferred from $|\psi_a\rangle$ to $|\Psi_3\rangle$ if $E = -1$ eV or to $|\Psi_4\rangle$ if $E = 1$ eV. At these energies, the oscillation amplitude of $\mathscr{C}_b(t)$ remains very weak and an amplitud-related interference appears in the $T(E)$ line shape.

The degenerancies at $E = \pm 1$ eV lead to a competition between a resonant and an interfering pathway at each of these energies. In the tunnelling regime, the interactions between the electrodes and the system are not strong enough to split significantly the two degenerate states. During the temporal evolution, the initial population then splits between the two pathways. A resonance involving half of the initial population is then observed on the target state. This explains why $T(E = \pm 1$ eV) is lower than 1 in the tunelling regime. Increasing the interactions between the electrodes and the system splits the degenerancies at $E = \pm 1$ eV, suppressing the competition between the resonant and interfering pathways. The amplitude-related interference is not screened by a resonance and clearly appears on the $T(E)$ profile. The same situation is observed in the ortho-configuration but not in the para-configuration, where $|\Psi_3\rangle$ and $|\Psi_4\rangle$ are disconnected from both electrodes.

Other interference patterns appear in Figure 8. The Dyson expansion of the time-dependent Schrodinger equation allows one to express the functions $\mathscr{C}_{\Psi_n} = \langle \Psi_n | \psi(t) \rangle$ and provide a simple explanation of these interference patterns. These functions read

$$\mathscr{C}_{\Psi_n}(t) \simeq \frac{h_{an}}{\omega_n}(1 - e^{i\omega_n t})e^{-iEt} \tag{36}$$

with $h_{aj} = \langle \psi_a | \mathscr{H} | \Psi_j \rangle$. As before, $\omega_j = E - \lambda_j$, where λ_j is the jth eigenvalue of the benzene ring. The expression of the target state amplitude probability is then given by

$$\mathscr{C}_b(t) \simeq -\sum_{n=1}^{6} \frac{h_{an}h_{nb}}{\omega_n}\left[\frac{1 - e^{i\omega_n t}}{\omega_n} + it\right] e^{-iEt} \tag{37}$$

with $h_{nb} = \langle \Psi_n | \mathscr{H} | \psi_b \rangle$. As for the dimer system, the term $\sum_n (h_{an}h_{nb}/\omega_n)t$ is the first order in the Taylor expansion of $\sin(\sum_n (h_{an}h_{nb}/\omega_n)t)$; its oscillation frequency is given by $\Omega(E) \simeq \sum_n (h_{an}h_{nb}/\omega_n)$. The expression of $\Omega(E)$ in the ortho and meta configurations is

$$\Omega_O(E) = \frac{1}{6}(\tau_1 + \tau_2 - \tau_4 - \tau_6) = -\frac{\vartheta^2(E^2 - 2)}{\Pi_n(E - \lambda_n)} \tag{38}$$

$$\Omega_M(E) = \frac{1}{6}(\tau_1 - \tau_2 - \tau_4 + \tau_6) = \frac{\vartheta^2 E}{\Pi_n(E - \lambda_n)} \tag{39}$$

with $\tau_i = \vartheta^2/(E - \lambda_i)$. The interferences located at $E = \pm(2)^{1/2}$ and $E = 0$ for the ortho- and meta-configuration, respectively, are consequently frequency-related interference as observed in the transverse configuration of the dimer system. This assertion is verified numerically in Figure 7b, where $|\mathscr{C}_b(t)|^2$ for the meta-configuration remains null when $E = 0$. The ortho-configuration is particularly interesting, since at $E = \pm(2)^{1/2}$ the oscillation frequencies of the $\mathscr{C}_{\Psi_n}(t)$ are not even commensurable with each other and yet an interference is obtained on $\mathscr{C}_b(t)$. This emphasizes the non-necessity for phase matching between the oscillation on the molecular states to obtain an interference pattern.

Thanks to the preliminary study of the single impurity and the dimer system, the interpretation of the $T(E)$ profile for the benzene ring becomes extremely easy, since it is a simple superposition of resonances and frequency- or amplitude-related interferences. The method presented in this article gives a rather simple physical explanation of the process involved in a molecular junction and can easily be applied to larger molecules. Very different conclusions relative to the origin of interference patterns in a benzene ring have recently been drawn.[43] On the basis of the Green function element beween the two carbons atoms connected to the elecrodes, rather than between states inside the two electodes, this analysis leads to different classification for the interference patterns. The interferences located at $E = \pm 1$ eV and $\pm(2)^{1/2}$ eV form the first class of interference, labeled multipath zeroes. The remaining interference, located at $E = 0$ eV in the meta configuration, is referred to as a resonance zero. The former are related to interfering spatial pathways in the molecule, whereas the latter requires a pole in the self-energy of

dx.doi.org/10.1021/jp111384d |J. Phys. Chem. B 2011, 115, 5582–5592

one of the pathways. Despite this strong difference of interpretation, the spectra obtained by both methods agree perfectly.

V. CONCLUSION

Good agreement has been demonstrated between the time-dependent method used in this article and well accepted time-independent calculations of the electronic transmission coefficient. The time-dependent method allows us to grasp the intrinsic phenomena taking place inside the junction. The resonances are interpreted as high frequency oscillations between eigenstates of the electrodes leading to a maximal transfer probability. Interference can have several origins: it can be frequency-related interferences where the oscillation frequency of $|\mathcal{C}_b(t)|^2$ cancel out or amplitude-related interference where the oscillation amplitude of $|\mathcal{C}_b(t)|^2$ drops drastically. To obtain a frequency-related interference, it is not necessary for the population of the molecular eigenstates to oscillate in phase, out of phase, or with any phase relation. Only the amplitude of these oscillations and the interaction of each molecular eigenstate with the $|\psi_b\rangle$ are relevant. The amplitude-related interferences require the presence of a dangling eigenstate only connected to one electrode. In such a case, the initial population is entirely transferred from $|\psi_a\rangle$ to this eigenstate and the oscillation amplitude of $|\mathcal{C}_b(t)|^2$ remains very low. We have also shown that in most of the cases the population of the molecular states remains almost null as expected in the super exchange picture of the tunnelling process. However, at resonance and for extremely weak interactions between the electrodes and the central system, these states are significantly populated and electron−electron interactions should be considered. This approach can now be generalized taking into account these electron interactions or inelastic effects[71,72] occurring in the junction.

AUTHOR INFORMATION

Corresponding Author

*E-mail: n-renaud@northwestern.edu (N.R.); ratner@northwestern.edu (M.A.R.); joachim@cemes.fr (C.J.).

ACKNOWLEDGMENT

This article is in honor of Shaul Mukamel, scientist, friend, scholar,and teacher. N.R. and C.J. would like to thank the E. U. Commission and the Japan's ministry of education, culture, sports, science and technology (MEXT) for their financial support through, respectively, the ICT PICO-INSIDE integrated project and the WPI MANA program. N.R. was supported as part of the Non-Equilibrium Energy Research Center (NERC), an Energy Frontier Research Center funded by the U.S. Department of Energy, Office of Science, Office of Basic Energy Sciences under Award Number DE-SC0000989.

REFERENCES

(1) Cuevas, J. C. *Molecular Electronics: An Introduction to Theory and Experiment*; World Scientific Series in Nanotechnology and Nanoscience; 2010.
(2) Aviram, A.; Ratner, M. A. *Chem. Phys. Lett.* **1974**, *29*, 227.
(3) Ashwell, G. J.; Sambles, J. R.; Martin, A. S.; Parker, W. G.; Szablewski, M. *J. Chem. Soc., Chem. Commun.* **1990**, *19*, 1374.
(4) Metzger, R. M. *Chem. Rev.* **2003**, *103*, 3803.
(5) Carter, F. L. *Physica D* **1984**, *10*, 175.
(6) Aviram, A. *J. Am. Chem. Soc.* **1988**, *110*, 5687.
(7) Joachim, C.; Gimzewski, J. K.; Aviram, A. *Nature* **2000**, *408*, 541.
(8) Ellenbogen, J. C.; Love, J. C. *Proc. IEEE* **2000**, *88*, 386.
(9) Remacle, F.; Levine, R. D. *J. Chem. Phys.* **2001**, *114*, 1039.
(10) Remacle, F.; Levine, R. D. *Phys. Rev. A* **2006**, *73*, 033820.
(11) Duchemin, I.; Joachim, C. *Chem. Phys. Lett.* **2005**, *406*, 167.
(12) Duchemin, I.; Renaud, N.; Joachim, C. *Chem. Phys. Lett.* **2008**, *452*, 269.
(13) Renaud, N.; Joachim, C. *Phys. Rev. A* **2008**, *78*, 062316.
(14) Renaud, N.; Ito, M.; Shangguan, W.; Saeys, M.; Hliwa, M.; Joachim, C. *Chem. Phys. Lett.* **2009**, *472*, 74.
(15) Nitzan, A. *Annu. Rev. Phys. Chem.* **2001**, *52*, 681.
(16) Drakova, D. *Rep. Prog. Phys.* **2001**, *64*, 205.
(17) Lippmann, B. A.; Schwinger, J. *Phys. Rev.* **1950**, *79*, 469.
(18) Buttiker, M.; Imry, Y.; Landauer, R.; Pinhas, S. *Phys. Rev. B* **1985**, *31*, 6207.
(19) Sautet, P.; Joachim, C. *Phys. Rev. B* **1988**, *38*, 12238.
(20) Ami, S.; Joachim, C. *Phys. Rev. B* **2002**, *65*, 155419.
(21) English, R. A.; Davison, S. G. *Phys. Rev. B* **1994**, *49*, 8718.
(22) Villagomez, C.; Zambelli, T.; Gauthier, S.; Gourdon, A.; Barthes, C.; Stojkovic, S.; Joachim, C. *Chem. Phys. Lett.* **2007**, *450*, 107.
(23) Villagomez, C.; Zambelli, T.; Gauthier, S.; Gourdon, A.; Stojkovic, S.; Joachim, C. *Surf. Sci.* **2009**, *603*, 1526.
(24) Bellec, A.; Ample, F.; Riedel, D.; Dujardin, G.; Joachim, C. *Nano Lett.* **2009**, *9*, 144.
(25) Mujica, V.; Kemp, M.; Ratner, M. A. *J. Chem. Phys.* **1994**, *101*, 6849.
(26) Mujica, V.; Kemp, M.; Ratner, M. A. *J. Chem. Phys.* **1994**, *101*, 6856.
(27) Mujica, V.; Kemp, M.; Roitberg, A.; Ratner, M. A. *J. Chem. Phys.* **1996**, *104*, 7296 .
(28) Datta, S. *Quantum Transport: Atom to Transistor*; Cambridge University Press: 2005. Datta, S. *Electronic Transport in Mesoscopic Systems*; Cambridge University Press: 1995.
(29) Pendry, J. B.; Pretre, A. B.; Krutzen, B. C. H. *J. Phys.: Condens. Matter* **1991**, *3*, 4313.
(30) Todorov, T. N.; Briggs, G. A. D.; Sutton, A. P. *J. Phys.: Condens. Matter* **1993**, *5*, 2389.
(31) Nieminen, J.; Niemi, E.; Rieder, K. H. *Surf. Sci. Lett.* **2004**, *552*, L47.
(32) Samanta, M. P.; Tian, W.; Datta, S. *Phys. Rev. B* **1996**, *53*, R7626.
(33) Tian, W.; Datta, S.; Hong, S.; Reifenberger, R.; Henderson, J. I.; Kubiak, C. P. *J. Chem. Phys.* **1998**, *109*, 2874.
(34) Heurich, J.; Cuevas, J. C.; Wenzel, W.; Schon, G. *Phys. Rev. Lett.* **2002**, *88*, 256803.
(35) Cuevas, J. C.; Heurich, J.; Pauly, F.; Wenzel, W.; Schon, G. *Nanotechnology* **2003**, *14*, R29.
(36) Nieminem, J.; Lahti, S.; Paavilainen, S.; Morgenstern, K. *Phys. Rev. B* **2002**, *66*, 165421.
(37) Cerda, J.; Van Hove, M. A.; Sautet, P.; Salmeron, M. *Phys. Rev. B* **1997**, *56*, 15885.
(38) Pickup, B.; Fowler, P. *Chem. Phys. Lett.* **2008**, *459*, 198.
(39) Ernzerhof, M.; Bahmann, H.; Goyer, F.; Zhuang, M.; Rocheleau, P. *J. Chem. Theor. Comput.* **2006**, *2*, 1291.
(40) Sautet, P.; Joachim, C. *Chem. Phys. Lett.* **1998**, *153*, 511.
(41) Solomon, G. C.; Andrews, D. Q.; Van Duyne, R. P.; Ratner, M. A. *J. Am. Chem. Soc.* **2008**, *130*, 7788.
(42) Capasso, F.; Datta, S. *Phys. Today* **1990**, 74.
(43) Hansen, T.; Solomon, G. C.; Andrews, D. Q.; Ratner, M. A. *J. Chem. Phys.* **2009**, *131*, 194704.
(44) Solomon, G. C.; Andrews, D. Q.; Hansen, T.; Goldsmith, R. H.; Wasielewski, M. R.; Van Duyne, R. P.; Ratner, M. A. *J. Chem. Phys.* **2008**, *129*, 054701.
(45) Yeganeh, S.; Ratner, M. A.; Mujica, V. *J. Chem. Phys.* **2007**, *126*, 161103.
(46) Nitzan, A. *J. Phys. Chem. A* **2001**, *105*, 2677.
(47) Solomon, G. C.; Hermann, C.; Hansen, T.; Mujica, V.; Ratner, M. A. *Nat. Chem.* **2010**, *2*, 223.

(48) Bar-Joseph, I.; Gurvitz, S. A. *Phys. Rev. B* **1991**, *44*, 3332.
(49) Ness, H.; Fisher, A. *Phys. Rev. B* **1997**, *56*, 12469.
(50) Sanchez, C.; Stamenova, M.; Sanvito, S.; Bowler, D. R.; Horsfield, A. P.; Todorov, T. N. *J. Chem. Phys.* **2006**, *124*, 214708.
(51) Subotnik, J.; Hansen, T.; Ratner, M. A.; Nitzan, A. *J. Chem. Phys.* **2009**, *130*, 144105.
(52) Stratford, K.; Beeby, J. L. *J. Phys.: Condens. Matter* **1993**, *5*, L289.
(53) Doyen, G. *J. Phys.: Condens. Matter* **1995**, *5*, 3305.
(54) Joachim, C.; Ratner, M. A. *Proc. Nat. Am. Soc.* **2005**, *102*, 8801.
(55) Remacle, F.; Levine, R. D. *Faraday Discuss.* **2006**, *131*, 45.
(56) Maciejko, J.; Wang, J.; Guo, H. *Phys. Rev. B* **2006**, *74*, 085324.
(57) Harbola, U.; Esposito, M.; Mukamel, S. *Phys. Rev. B* **2006**, *74*, 235309.
(58) Fano, U. *Phys. Rev. B* **1961**, *124*, 1866.
(59) Fano, U.; Rau, A. R. P.; Academic: Orlando, FL, 1986.
(60) Mies, F. H. *Phys. Rev.* **1968**, *175*, 164.
(61) Durand, Ph.; Paidarova, I.; Gadea, F. X. *J. Phys. B* **2001**, *34*, 1953.
(62) Durand, Ph.; Paidarova, I. *J. Phys. B* **2002**, *35*, 469.
(63) Bloch, C. *Nucl. Phys.* **1958**, *6*, 329.
(64) Durand, Ph. *Phys. Rev. A* **1983**, *28*, 3184.
(65) Joachim, C.; Launay, J. P. *Chem. Phys.* **1986**, *109*, 93.
(66) Gurvitz, S. A.; Kalbermann, G. *Phys. Rev. Lett.* **1987**, *59*, 262.
(67) Reuter, M. G.; Hansen, T.; Seidman, T.; Ratner, M. A. *J. Phys. Chem. A* **2009**, *113*, 4665.
(68) Bardeen, J. *Phys. Rev. Lett.* **1961**, *6*, 57.
(69) Skourtis, S. S.; Mukamel, S. *Chem. Phys.* **1995**, *7*, 367.
(70) Solomon, G. C.; Andrews, D. Q.; Van Duyne, R. P.; Ratner, M. A. *ChemPhysChem* **2009**, *10*, 257.
(71) Sergueev, N.; Demkov, A. A.; Guo, H. *Phys. Rev. B* **2007**, *75*, 233418.
(72) Seideman, T.; Guo, H. *J. Theor. Comput. Chem.* **2004**, *2*, 439.